

Photoinduced Electron-Transfer Processes Based on Novel Bipyridine–Ru(II) Complex: Properties of *cis*-[Ru(2,2'-bipyridine)₂(5,6-bis(3-amidopyridine)-7-oxanorbornene)](PF₆)₂ and *cis*-[Ru(2,2'-bipyridine)₂(3-aminopyridine)](PF₆)₂ Complexes

Simone D. Inglez,[†] Francisco C. A. Lima,[†] Albérico B. F. Silva,[†] Andreza R. Simioni,[‡] Antônio C. Tedesco,[‡] Juliana F. S. Daniel,[§] Benedito S. Lima-Neto,^{*,†} and Rose M. Carlos^{*,§}

Instituto de Química de São Carlos, Universidade de São Paulo, CP 780, 13650-970 São Carlos, SP, Brasil, Faculdade de Filosofia Ciências e Letras de Ribeirão Preto, Universidade de São Paulo, Ribeirão Preto, SP, Brasil, and Departamento de Química, Universidade Federal de São Carlos, CP 676, 13565-905 São Carlos, SP, Brasil

Received December 27, 2006

This paper presents the synthesis, MO calculations, and photochemical and photophysical properties of *cis*-[Ru(bpy)₂(3Amdpy₂oxaNBE)](PF₆)₂ (**2**), where bpy is 2,2'-bipyridine and 3Amdpy₂oxaNBE is the novel 5,6-bis(3-amidopyridine)-7-oxanorbornene chelate-ligand (**1**). Complex **2** is considered in relation to the *cis*-[Ru(bpy)₂(3Amnpy)](PF₆)₂ (**3**) analogous complex, where 3Amnpy is 3-aminopyridine. Complexes **2** and **3** exhibit absorptions near 350 nm and in the 420–500 nm region attributable to a contribution from MLCT transitions ($d_{\pi} \rightarrow \text{bpy}$ and $d_{\pi} \rightarrow \text{L}$; L = 3Amdpy₂oxaNBE or 3Amnpy). Whereas complex **3** is photochemically reactive, complex **2** shows luminescence either at 77 K or at room temperature in fluid solution. The emission of **2** assignable as an MLCT (Ru \rightarrow bpy) emission is characterized by a long lifetime at room temperature (650 ns in CH₃CN and 509 ns in H₂O). It is independent of λ_{irr} , but it is temperature dependent; i.e., it increases as the temperature is lowered. Considering the chelate ring of **1** contributes to the stability of the complex **2** under continuous light irradiation, the difference in the primary photoprocesses of **3** (loss of 3Amnpy) and **2** (luminescence) may be caused by a lowering of the lowest excited state from **3** to **2**. The surface crossing to the lowest MC state value of 987 cm⁻¹ (similar to that of [Ru(bpy)₃]²⁺) will be prevented in the case of complex **2**, and as a result, efficient 3Amdpy moiety loss cannot occur. The electronic depopulation of the {Ru(bpy)₂} unit and population of a bpy* orbital upon excitation are evident by comparing the photophysical properties with those of a [Ru(bpy)₃]²⁺ related complex. Moreover, a reduction of a bpy ligand in the MLCT excited state is indicated by time-resolved spectra that show features typical of bpy*-. The photocatalytic property of **2** is spectroscopically demonstrated by oxidative quenching using either methylviologen²⁺ or [RuCl(NH₃)₅]²⁺ electron-acceptor ions.

Introduction

The design and synthesis of electron donor- and acceptor-photosensitizer arrays have attracted considerable attention as they have potential application in photoelectric molecular devices, catalysts, and biomimetic chemistry.^{1–3} In particular,

by combining inorganic photochemistry with conducting polymers, it is possible to create “molecular wires” that interconnect multiple chromophores and quenchers within a

* To whom correspondence should be addressed. E-mail: benedito@iqsc.usp.br (B.S.L.-N.); rosem@dq.ufscar.br (R.M.C.).

[†] Instituto de Química de São Carlos.

[‡] Faculdade de Filosofia Ciências e Letras de Ribeirão Preto.

[§] Universidade Federal de São Carlos.

(1) Balzani, V.; Credi, A.; Raymo, F. M.; Stoddart, J. F. *Angew. Chem., Int. Ed.* **2000**, *39*, 3348–3391.

(2) (a) Loiseau, F.; Marzanni, G.; Quici, S.; Indelli, M. T.; Campagna, S. *Chem. Commun.* **2003**, 286–287. (b) Abrahamsson, M. L. A.; Baudin, H. B.; Tran, A.; Philouse, C.; Berg, K. E.; Raymond-Johansson, M. K.; Sun, L.; Akermark, B.; Styring, S.; Hammarstrom, L. *Inorg. Chem.* **2002**, *41*, 1534–1544.

(3) (a) Xu, Y. H.; Eilers, G.; Borgstrom, M.; Pan, J. X.; Abrahamsson, M.; Magnuson, A.; Lomoth, R.; Bergquist, J.; Polivka, T.; Sun, L. C.; Sundstrom, V.; Styring, S.; Hammarstrom, L.; Akermark, B. *Chem—Eur. J.* **2005**, *11*, 7305–7314. (b) Ballardini, R.; Balzani, V.; Credi, A.; Gandolfi, M. T.; Venturi, M. *Acc. Chem. Res.* **2001**, *34*, 445–455.

single molecular framework.⁴ A strategy is to develop ligands connected to cyclic olefin which is subjected to ring opening metathesis polymerization (ROMP).⁵

We have examined olefin–polypyridyl Ru(II)-based compounds that could generate molecular wires, where the monomer-ligand 5,6-bis(3-amidopyridine)-7-oxanorbornene (**1**; 3Ampdy₂oxaNBE), synthesized from the reaction between 3-aminopyridine (3Ampny) and hydrolyzed *exo*-7-oxabicyclo[2.2.1]hept-5-ene-2,3-dicarboxylic anhydride (oxaNBE), reacts with *cis*-[RuCl₂(bpy)₂] affording the *cis*-[Ru(bpy)₂(3Ampdy₂oxaNBE)](PF₆)₂ complex (**2**). The optical absorption, characterization, and photochemical and photophysical properties of this novel complex and the related *cis*-[Ru(bpy)₂(3Ampny)₂](PF₆)₂ complex (**3**) were studied. The results were examined to discover like and unlike characteristics between **2** and **3**, observing the benefits of the 7-oxanorbornene moiety in the derivatized monomer-ligand. The results were also examined in relation to the [Ru(bpy)₃](PF₆)₂ complex, and MO calculations of **2** were performed.

The choice of 2,2'-bipyridine complexes of Ru(II) is attractive since the related [Ru(bpy)₃]²⁺ complex ion is the most well-known and thoroughly studied photosensitizer.^{6,7} Because of its octahedral coordination geometry, its derivatives have been extensively investigated, where a specific ligand can be introduced in a controlled manner to tune the photophysical, photochemical, and electrochemical properties.^{1–4,8} Moreover, many ruthenium complexes connected to norbornene derivatives reported to date⁵ contain pyridine-based ligands as bridge.

Experimental Section

General. All reactions were performed under argon atmosphere unless otherwise stated. All chemicals used were of reagent grade or comparable purity. RuCl₃·*x*H₂O and [Ru(bpy)₃]Cl₂·6H₂O from Strem; *exo*-7-oxabicyclo[2.2.1]hept-5-ene-2,3-dicarboxylic anhydride from Aldrich; 2,2'-bipyridine (bpy), 3-aminopyridine (3Ampny), lithium chloride, sucrose, and ammonium hexafluorophosphate from Aldrich; tetrabutylammonium hexafluorophosphate (TBAPF₆) from Fluka; and thionyl chloride (SOCl₂) from Merck were used as acquired. HPLC grade acetonitrile and dichloromethane were distilled prior to use. *cis*-[RuCl₂(bpy)₂]·2H₂O (Anal. Calcd for RuC₂₀H₁₆N₄Cl₂·2H₂O: C, 46.14; H, 3.84; N, 10.76. Found: C,

46.37; H, 3.39; N, 10.71%) and *cis*-[Ru(bpy)₂(3Ampny)₂](PF₆)₂·1H₂O (**3**; Anal. Calcd for RuC₃₀H₂₈N₈P₂F₁₂·1H₂O: C, 39.59; H, 3.22; N, 12.17. Found: C, 39.61; H, 3.30; N, 12.31%) were prepared according to the literature methods.^{9,10}

Synthesis of 5,6-Bis(3-amidopyridine)-7-oxanorbornene (1**; 3Ampdy₂oxaNBE).** The *exo*-7-oxabicyclo[2.2.1]hept-5-ene-2,3-dicarboxylic anhydride compound (1.0 g, 6.0 mmol) was quantitatively hydrolyzed in 5 mL of water and evaporated to dryness. The isolated monomer (1.0 g; 5.4 mmol) was suspended in 5 mL of dichloromethane and mixed with redistilled SOCl₂ (1.0 mL; 14 mmol). The resulting mixture was stirred for 2 h under reflux, and, thus, evaporated to dryness. The solid was washed with anhydrous benzene and dichloromethane and dried under vacuum (30% yield). ¹³C NMR (CD₃CN), δ ppm: 50.15, 83.41, 137.93, 170.0. A 0.25 g portion of the obtained compound (1.1 mmol) was dissolved in 10 mL of acetone, and 3-aminopyridine (0.21 g; 3.3 mmol) dissolved in 5 mL of acetone was added. The mixture was then refluxed for 2 h and cooled to room temperature, and the precipitate was filtered, washed with acetone, and dried under vacuum (88% yield). ¹H NMR (DMSO-*d*₆), δ ppm: 6.53 (q, 2H), 7.49 (dd, 2H, *J*₁ = 4.7 Hz, *J*₂ = 8.28 Hz), 8.16 (dd, 2H, *J*₁ = 2.3 Hz, *J*₂ = 8.28 Hz), 8.41 (dd, 2H, *J*₁ = 1.4 Hz, *J*₂ = 4.7 Hz), 8.88 (d, 2H, *J* = 2.4 Hz). ¹³C NMR (DMSO-*d*₆), δ ppm: 47.08, 79.34, 79.37, 123.77, 126.56, 131.77, 136.80, 141.13, 144.80, 172.60. Anal. Calcd for C₁₈H₁₆O₃N₄·3H₂O: C, 55.07; H, 5.64; N, 14.33. Found: C, 56.06; H, 5.53; N, 14.52%.

Synthesis of *cis*-[Ru(bpy)₂(3Ampdy₂oxaNBE)](PF₆)₂ (2**).** *cis*-[RuCl₂(bpy)₂]·2H₂O (0.20 g; 0.38 mmol) was dissolved in a 1:1 EtOH/H₂O mixture (10 mL), and an amount of **1** (0.13 g; 0.38 mmol) was added. The solution was stirred under argon atmosphere for 8 h under reflux. The volume was reduced to approximately 1 mL, and a stoichiometric amount of NH₄PF₆ was added to precipitate the complexes. A reddish-brown precipitate that formed for *cis*-[Ru(bpy)₂(3Ampdy₂oxaNBE)](PF₆)₂ (**2**) was filtered, washed with water and diethyl ether, and dried under vacuum (55% yield). ¹H NMR (DMSO-*d*₆), δ ppm: 3.45 (q, 2H, *J*₁ = 7.02 Hz, *J*₂ = 14 Hz), 4.16 (q, 2H, *J*₁ = 7.18 Hz, *J*₂ = 14 Hz), 4.44 (2H), 6.40 (q, 2H), 7.13 (m, 2H), 7.24 (d, 1H, *J* = 6.9 Hz), 7.73 (d, 1H, *J* = 6.0 Hz), 7.79 (dd, 4H, *J*₁ = 4.9 Hz, *J*₂ = 8 Hz), 8.05 (dd, 2H, *J*₁ = 1.3 Hz, *J*₂ = 8 Hz), 8.32 (m, 2H), 8.38 (m, 1H), 8.47 (m, 1H), 8.75 (m, 2H), 8.97 (d, 2H, *J* = 6.47 Hz), 9.38 (dt, 2H, *J* = 5.34 Hz), 9.93 (d, 2H, *J* = 5.51 Hz), 9.95 (d, 2H, *J* = 5.99 Hz). ¹³C NMR (DMSO-*d*₆), δ ppm: 48.28, 81.45, 123.31, 125.61, 126.30, 126.89, 127.75, 131.63, 134.90, 135.75, 136.47, 167.00. *ν*_{CO} 1721, 1687 cm⁻¹; *ν*_{NH} 3100, 3051 cm⁻¹. Anal. Calcd for RuC₃₈H₃₆N₈O₃P₆F₁₂·H₂O: C, 42.98; H, 3.58; N, 10.55%. Found: C, 43.07; H, 3.51; N, 10.43.

Instrumentation. Optical spectra were recorded on a Varian model Cary 500 NIR spectrophotometer, using 1 cm path length quartz cells. The FTIR spectra were measured in KBr pellets on a Bomem-Michelson 102 spectrometer in the 4000–400 cm⁻¹ region. ¹H and ¹³C NMR spectra were measured in a CD₃CN solution using a BRUKER AC-200 system with tetramethylsilane as internal standard. CHN elemental analyses were performed on an EA 1110 CHNS-O Carlo Erba Instrument in the Microanalytical Laboratory at Universidade de São Paulo, São Carlos (SP). Cyclic voltammetry was performed on a Microquímica model MGPG-01 potentiostat. This instrument was also used for the characterization of the complexes. In the electrochemical experiments, the working and

(4) (a) Pautzsch, T.; Blankenburg, L.; Klemm, E. *J. Polym. Sci., Part A: Polym. Chem.* **2004**, *42*, 722–732. (b) Barigelletti, F.; Flamigni, L. *Chem. Soc. Rev.* **2000**, *29*, 1–12. (c) James, D. K.; Tour, J. M. *Molecular Wires and Electronics*; Würthner, F. Ed.; Topics in Current Chemistry 257; Springer-Verlag: Berlin, 2005; pp 33–62.

(5) (a) Rezvani, A.; Bazzi, H. S.; Chen, B. Z.; Rakotondrandany, F.; Sleiman, H. F. *Inorg. Chem.* **2004**, *43*, 5112–5119. (b) Chen, B. Z.; Sleiman, H. F. *Macromolecules* **2004**, *37*, 5866–5872. (c) Carlise, J. R.; Weck, M. *J. Polym. Sci., Part A: Polym. Chem.* **2004**, *42*, 2973–2984. (d) Chen, B. Z.; Metera, K.; Sleiman, H. F. *Macromolecules* **2005**, *38*, 1084–1090.

(6) Juris, A.; Balzani, V.; Barigelletti, F.; Campagna, S.; Belser, P.; Von Zelewsky, A. *Coord. Chem. Rev.* **1988**, *84*, 85–277.

(7) Kalyanasundaram, K. *Photochemistry of Polypyridine and Porphyrin Complexes*; Academic Press: London, 1992.

(8) (a) Wu, X.; Fraser, C. L. *Macromolecules* **2000**, *33*, 4053–4060. (b) Wu, X.; Fraser, C. L. *Macromolecules* **2000**, *33*, 7776–7785. (c) Smith, A. P.; Fraser, C. L. *J. Polym. Sci., Part A: Polym. Chem.* **2002**, *40*, 4250–4255. (d) Smith, A. P.; Fraser, C. L. *Macromolecules* **2003**, *36*, 5520–5525. (e) Fitz-Gerald, J. M.; Jennings, G.; Johnson, R.; Fraser, C. L. *Appl. Phys. A* **2005**, *80*, 1109–1113.

(9) Sullivan, B. P.; Salmon, D. J.; Meyer, T. J. *Inorg. Chem.* **1978**, *17*, 3334–3341.

(10) Ellis, C. D.; Margerum, L. D.; Murray, R. W.; Meyer, T. J. *Inorg. Chem.* **1983**, *22*, 1283–1291.

auxiliary electrodes were a stationary platinum foil and wire, respectively. The reference electrode was Ag/AgCl in a Luggin capillary. The measurements were taken at room temperature in freshly distilled CH₃CN containing 0.1 mol L⁻¹ of TBAPF₆.

Continuous Photolysis. Monochromatic irradiation at 400 nm was generated using a 200-W xenon lamp in an Oriel model 68805 universal arc lamp source selected with an appropriate interference filter (Oriel). The experiments were carried out at room temperature in 1.0 cm path length 4 side quartz cells capped with a rubber septum, and monitored by UV-vis spectrophotometry. The magnetically stirred solutions (~10⁻⁴–10⁻³ mol L⁻¹ initial complex concentration) were deoxygenated with dinitrogen. Potassium(tris-oxalate)ferrate(III), used in actinometry at 450 nm, was prepared according to Calvert and Pitts.¹¹

Luminescence and Quantum Yield Properties. Emission spectra at 25.0 °C were recorded on an Aminco-Bowman model J4-8960A spectrofluorometer, with a high-pressure xenon lamp and an IP 28 type photomultiplier. The corrected emission spectra were recorded using a Fluorolog 3 spectrofluorimeter from Ivon Jobin connected to an instrument setup file to correct the nonlinearity in the intensity of the excitation light and to adjust the detector sensitivity as a function of wavelength. The emission quantum yield was determined by comparison with a 10⁻⁴ mol L⁻¹ acetonitrile solution of [Ru(bpy)₃]²⁺ ($\phi_{em} = 0.062$) as a standard,¹² using equation $\phi_{em,S} = \phi_{em,R}(A_R/A_S)(I_S/I_R)(n_S/n_R)$, where A_S and A_R are the absorption values of sample and reference, I_S and I_R are the integrated emission intensity of sample and reference, and n_S and n_R are the refractive indices of sample and reference.¹³ The rate constants for radiative (k_r) and nonradiative (k_{nr}) decay are related to ϕ_{em} and τ_{em} by the following:¹⁴

$$k_r = \phi_{em}/\tau_{em} \quad (1)$$

$$k_{nr} = (1 - \phi_{em})/\tau_{em} \quad (2)$$

Quenching Experiments. Oxidative-quenching experiments of the excited complex were performed using *N,N'*-methyl-viologen chloride (methylviologen; MV²⁺) and [RuCl(NH₃)₅]Cl₂ as electron acceptor.¹⁴ At least 6 samples of the complex were prepared as aqueous solution, with MV²⁺ concentrations between 0 and 6 mmol L⁻¹, and 0 and 9 mmol L⁻¹ for [RuCl(NH₃)₅]Cl₂.

Stern–Volmer plots¹⁴ of the observed decrease in the emission intensity with an increase in the quencher concentration showed a good linear relation with an intercept of 1, so that the oxidative-quenching rate constant k_q could be calculated using eq 3 and the emission lifetime of the complex in the absence of quencher, τ_{em} :

$$I^0/I = 1 + k_q\tau_{em}[Q] \quad (3)$$

Luminescence Lifetimes and Kinetic Experiments. Time-correlated single-photon counting (TCSPC) was used to determine the fluorescence lifetimes. This is a widely used technique and has been extensively reviewed.¹⁵ The apparatus comprised a frequency-doubled mode locked Nd:YAG laser (Coherent Antares 764) which synchronously pumped a cavity-dumped dye laser (Coherent 701-3CD) with a medium gain of either Rhodamine 6G or DCM (4-

dicyanomethylene-2-methyl-6-(*p*-dimethylaminostyryl)-4*H*-pyran). It produced a 3.8 MHz train of pulses with full width at half-maximum (fwhm) of 6 ps and an average power of 1040 mW in the 300–800 nm range. The fluorescence emission was collected at 90°, and the emission wavelength was selected by a double-beam monochromator. A Hamamatsu 1564-UO1 microchannel plate was used to detect the fluorescence emission, together with standard discriminators, time to amplitude converter (TAC), and a multi-channel analyzer (Canberra 35), giving typical instrument response times of 50 ps (fwhm). All the decays were recorded to a minimum of 20000 counts in the channel of maximum intensity, and analyzed by iterative deconvolution and nonlinear least-squares fitting. The fits were validated by the reduced χ -squared, visually random residuals, and autocorrelation functions.

Time-resolved optical (TRO) spectra were obtained using a laser flash-photolysis apparatus containing a Continuum Q-switched Nd:YAG laser (Continuum, Santa Clara, CA) with excitation provided by the third harmonic at $\lambda = 355$ nm. The pulse length was 8 ns, the beam diameter incident on sample was 6 mm, and the repetition rate was 10 Hz. The laser pulse was set up from 15 mJ per pulse in the photobleaching studies measured with a Field Master power meter with L-30V head. The growth-decay kinetics were measured at a single wavelength using a monochromator (M300 from Bentham) and a photomultiplier (Hamamatsu, model R928P). Transient decays were averaged using a Tetrax TDS 340A digital oscilloscope. The stored digitized kinetic decays were transferred to a personal computer (PC) for the analysis with software supplied by Edinburgh Instruments.

Theoretical Molecular Orbital Calculation. The calculations reported in this paper have been performed with the Gaussian 03 package.¹⁶ The starting molecular geometries were obtained at the UHF/3-21G level of theory. The final molecular geometry optimizations were performed using the Kohn–Sham density functional theory (DFT)¹⁷ with the Becke three-parameter hybrid exchange-correlation function known as B3LYP^{18,19} alone with the pseudo-potential basis set LanL2DZ.²⁰ No symmetry condition was imposed. Vibrational frequencies were calculated from analytic second derivatives to check the minimum on the potential energy surface. The natural bond orbital calculation was performed using the NBO 5.0 program,²¹ as implemented in the Gaussian 03 package.

- (16) Frisch, M. J.; Trucks, G. W.; Schlegel, H. B.; Scuseria, G. E.; Robb, M. A.; Cheeseman, J. R.; Montgomery, J. A., Jr.; Vreven, T.; Kudin, K. N.; Burant, J. C.; Millam, J. M.; Iyengar, S. S.; Tomasi, J.; Barone, V.; Mennucci, B.; Cossi, M.; Scalmani, G.; Rega, N.; Petersson, G. A.; Nakatsuji, H.; Hada, M.; Ehara, M.; Toyota, K.; Fukuda, R.; Hasegawa, J.; Ishida, M.; Nakajima, T.; Honda, Y.; Kitao, O.; Nakai, H.; Klene, M.; Li, X.; Knox, J. E.; Hratchian, H. P.; Cross, J. B.; Bakken, V.; Adamo, C.; Jaramillo, J.; Gomperts, R.; Stratmann, R. E.; Yazyev, O.; Austin, A. J.; Cammi, R.; Pomelli, C.; Ochterski, J. W.; Ayala, P. Y.; Morokuma, K.; Voth, G. A.; Salvador, P.; Dannenberg, J. J.; Zakrzewski, V. G.; Dapprich, S.; Daniels, A. D.; Strain, M. C.; Farkas, O.; Malick, D. K.; Rabuck, A. D.; Raghavachari, K.; Foresman, J. B.; Ortiz, J. V.; Cui, Q.; Baboul, A. G.; Clifford, S.; Cioslowski, J.; Stefanov, B. B.; Liu, G.; Liashenko, A.; Piskorz, P.; Komaromi, I.; Martin, R. L.; Fox, D. J.; Keith, T.; Al-Laham, M. A.; Peng, C. Y.; Nanayakkara, A.; Challacombe, M.; Gill, P. M. W.; Johnson, B.; Chen, W.; Wong, M. W.; Gonzalez, C.; Pople, J. A. *Gaussian 03*, revision C.02; Gaussian, Inc.: Wallingford, CT, 2004.
- (17) Kohn, W.; Sham, L. J. *Phys. Rev.* **1965**, *140*, A1133.
- (18) Lee, C.; Yang, W.; Parr, R. G. *Phys. Rev.* **1998**, *B 37*, 785–789.
- (19) Becke, A. D. *J. Chem. Phys.* **1993**, *98*, 5648–5652.
- (20) Hay, P. J.; Wadt, W. R. *J. Chem. Phys.* **1985**, *82*, 270–283. (b) Wadt, W. R.; Hay, P. J. *J. Chem. Phys.* **1985**, *82*, 284–298. (c) Hay, P. J.; Wadt, W. R. *J. Chem. Phys.* **1985**, *82*, 299–310.

(11) Calvert, J. G.; Pitts, J. N. *Photochemistry*, 2nd ed.; Wiley: New York, 1967; pp 779–789.

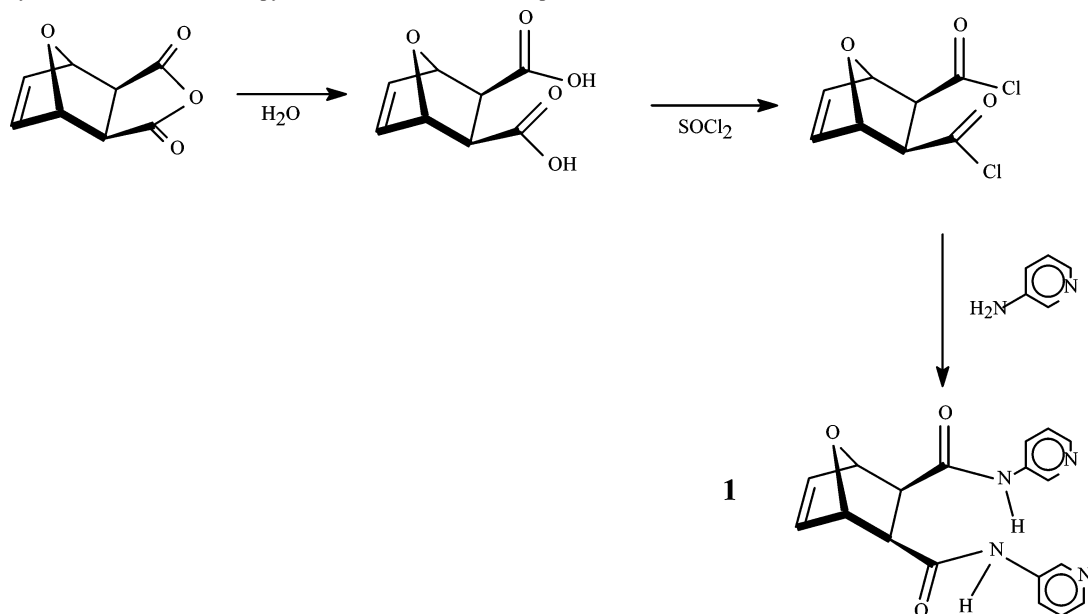
(12) (a) Caspar, J. V.; Meyer, T. J. *J. Am. Chem. Soc.* **1983**, *105*, 5583–5590.

(13) Calvert, J. M.; Caspar, J. V.; Binstead, R. A.; Westmoreland, T. D.; Meyer, T. J. *J. Am. Chem. Soc.* **1982**, *104*, 6620–6627.

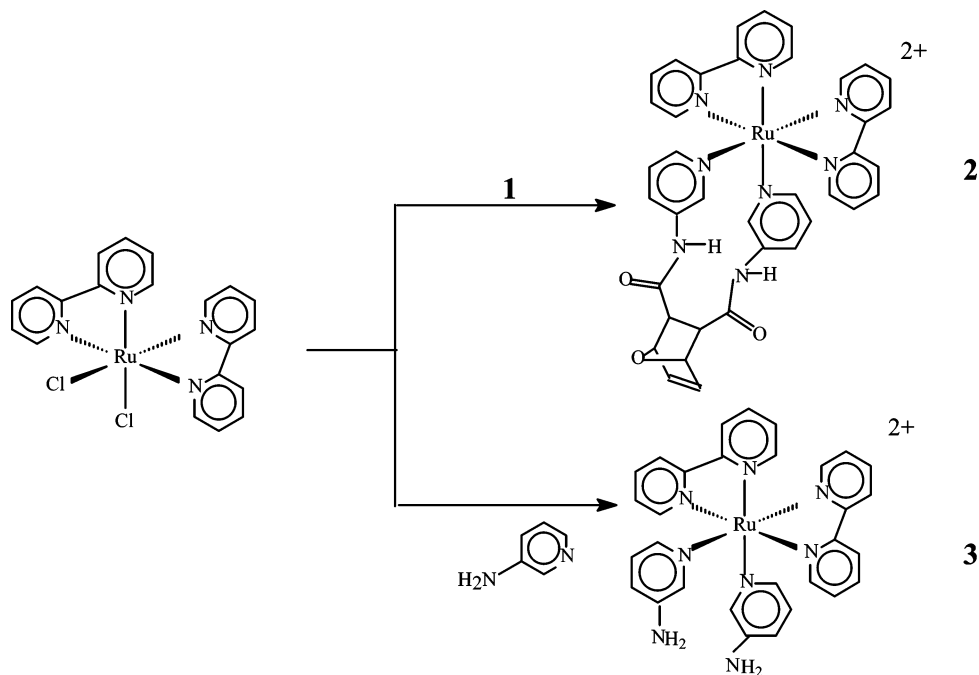
(14) Kavarnos, G. J.; Turro, J. N. *Chem. Rev.* **1986**, *86*, 401–449.

(15) Hungerford, G.; Birch, D. J. S. *Meas. Sci. Technol.* **1996**, *7*, 121–135.

Scheme 1. Synthesis of 5,6-Bis(3-amidopyridine)-7-oxanorbornene Compound (**1**)



Scheme 2. Syntheses of *cis*-[Ru(bpy)₂(3Amdpy₂oxaNBE)](PF₆)₂ (**2**) and *cis*-[Ru(bpy)₂(3Amnpy₂)](PF₆)₂ (**3**) Complexes



In order to analyze the metal–ligand interaction energies and the composition of the orbitals, we used fragments 3Amdpy₂-oxaNBE, bipyridine, and atom Ru. This means that the MOs are expanded in the converged molecular or atomic orbitals of these fragments. The Mulliken population of a fragment orbital in a molecular orbital is used to denote the percentage of a fragment orbital character of that molecular orbital. As a first approximation to excitation energies, the differences between one-electron energies of the appropriate virtual and occupied molecular orbital may be used.

(21) Glendening, E. D.; Badenhop, J. K.; Reed, A. E.; Carpenter, J. E.; Bohmann, J. A.; Bohmann, Morales, C. M.; Weichold, F. *NBO 5.0*; Theoretical Chemistry Institute, University of Wisconsin: Madison, WI, 2001.

Results and Discussion

Synthesis. The amine groups of 3-aminopyridine molecules were modified to amide functions via reaction with 7-oxanorbornene molecule modified by carbonyl functions, as illustrated in Scheme 1. The result is pyridine molecules connected via an amide-substituted-7-oxanorbornene unit (**1**). The pyridine units characterize a bidentate ligand which replaces the chloride ligands in the bis(bipyridine)–Ru(II) complex, as illustrated in Scheme 2, resulting in complex **2**. Complex **3** with two unconnected pyridine units was prepared as a reference material,¹⁰ which is similar to complex **2** (Scheme 2). Complexes **2** and **3** differ by the different azo-groups in the pyridine units, where in complex

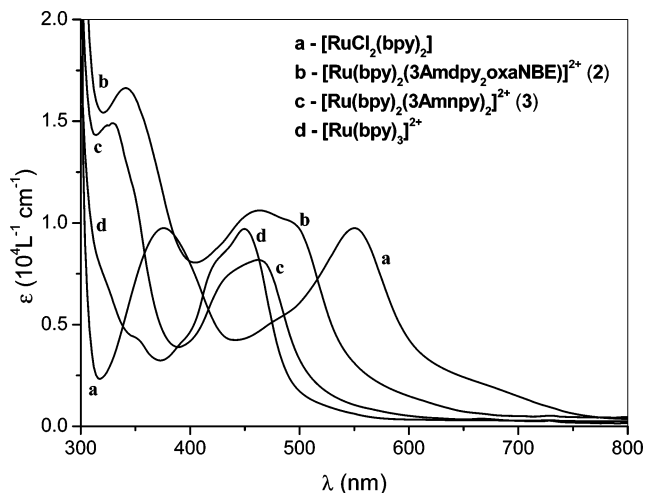


Figure 1. Electronic absorption spectra in deaerated CH_3CN solution.

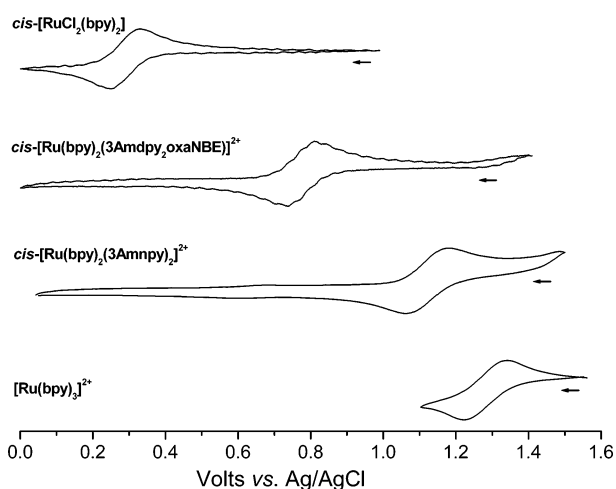


Figure 2. Cyclic voltammograms in deaerated CH_3CN solution ($[\text{Ru}] = 1 \text{ mmol L}^{-1}$, $25.0 \text{ }^\circ\text{C}$, 0.1 mol L^{-1} TBAPF₆, scan rate 100 mV s^{-1} , sensibility $50 \text{ } \mu\text{A}$).

2 an amide (amd) group is present while complex **3** has an amine (amn) group.

Complexes **2** is very stable in air and exhibits great tolerance to the usual organic solvents for several hours. It was characterized using elemental analysis, IR, and ^1H and ^{13}C NMR.

Electronic Absorption Spectra. The absorption spectra of complexes *cis*- $[\text{RuCl}_2(\text{bpy})_2]$, **2**, **3**, and $[\text{Ru}(\text{bpy})_3]^{2+}$ in CH_3CN solution are depicted in Figure 1. The absorption maxima and extinction coefficients relevant to this investigation are summarized in Table 1 and agree with the literature.^{10,22}

The absorption spectrum of **3** shows a band at 464 nm ($\epsilon_{\text{max}} = 8119 \text{ mol}^{-1} \text{ L cm}^{-1}$) with a shoulder around 431 nm , whereas the spectrum of **2** shows a band at 460 nm ($\epsilon_{\text{max}} = 10247 \text{ mol}^{-1} \text{ L cm}^{-1}$) with a shoulder around 498 nm .

Separate charge-transfer bands have been observed in a series of mixed-ligand complexes.^{6,23} The lowest energy

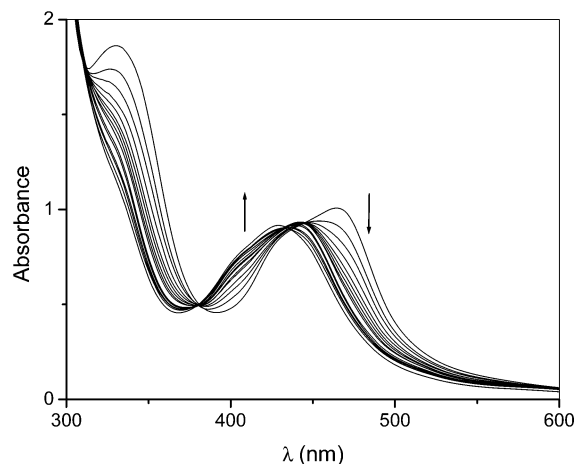


Figure 3. Electronic spectral changes resulting from the 440 nm photolysis of complex **3** (0.12 mmol L^{-1}) in deaerated CH_3CN solution.

absorptions usually correspond to promotion of an electron to the most easily reduced ligand. Figure 2 shows that, for $[\text{RuCl}_2(\text{bpy})_2]$, **2**, **3**, and $[\text{Ru}(\text{bpy})_3]^{2+}$, oxidations occur at $+0.33$, 0.81 , 1.16 , and 1.34 , and reductions occur at $+0.25$, 0.73 , 1.06 , and 1.23 versus Ag/AgCl electrode, respectively. Thus, in **2**, the absorption at 460 nm is assigned to the MLCT processes involving the *bpy* ligand, and the absorption at 498 nm belongs to CT transitions from $\text{Ru } d_{\pi}$ orbitals to the lowest π^* orbital of the $3\text{Amdpy}_2\text{oxaNBE}$ ligand. The differences in potential between the oxidations and reductions are related to the energy required to excite photochemically an electron from a metal d_{π} into a ligand π^* .^{14,24}

Figure 1 shows that attaching the 7-oxanorbornene molecule to the 3Amnpy ligand also has an influence on the position and relative intensity of the absorption band at 350 nm , which shifts to a longer wavelength and becomes weaker going from **2** to **3**. This spectroscopic behavior was observed earlier for $[\text{Ru}(\text{bpy})_2\text{LL}']^{2+}$ based complexes with chelating ligands.²⁵

Continuous Photolysis. The photolysis of complex **3** (0.12 mmol L^{-1} in CH_3CN) with 440 nm light led to a decrease of the characteristic absorption band at 464 nm (Figure 3) and the appearance of a new band at 426 nm ($\epsilon_{\text{max}} = \text{ca. } 7600 \text{ mol}^{-1} \text{ L cm}^{-1}$). The spectral changes at 446 and 434 nm suggest the occurrence of successive photoreactions.

The MLCT absorption bands of the related solvento *cis*- $[\text{Ru}(\text{bpy})_2(\text{pyridine})(\text{CH}_3\text{CN})]^{2+}$ ($\lambda_{\text{max}} = 440 \text{ nm}$; $\epsilon_{\text{max}} = 9700 \text{ mol}^{-1} \text{ L cm}^{-1}$) and *cis*- $[\text{Ru}(\text{bpy})_2(\text{CH}_3\text{CN})_2]^{2+}$ ($\lambda_{\text{max}} = 426 \text{ nm}$; $\epsilon_{\text{max}} = 8700 \text{ mol}^{-1} \text{ L cm}^{-1}$) complexes occur in the same spectral ranges observed for the photoproducts in the present case.²⁶ Thus, a possible explanation for the spectral changes would be a simple 3Amnpy photosolvation to form *cis*- $[\text{Ru}$

(22) Fergusso, J. E.; Harris, G. M. *J. Chem. Soc. A* **1966**, 1293–1296.

(23) (a) Rillema, D. P.; Allen, G.; Meyer, T. J.; Conrad, D. *Inorg. Chem.* **1983**, *22*, 1617–1622. (b) Barigelletti, F.; Juris, A.; Balzani, V.; Belsler, P.; von Zelewsky, A. *Inorg. Chem.* **1983**, *22*, 3335–3339.

(24) Yang, X. J.; Janiak, C.; Heinze, J.; Drepper, P. M.; Piotrowski, H.; Klufers, P. *Inorg. Chim. Acta* **2001**, *318*, 106–116.

(25) Root, M. J.; Sullivan, B. P.; Meyer, T. J.; Deutsch, E. *Inorg. Chem.* **1985**, *24*, 2731–2739.

(26) (a) Durham, B.; Walsh, J. L.; Carter, C. L.; Meyer, T. J. *Inorg. Chem.* **1980**, *19*, 860–865. (b) Pinnick, D. V.; Durham, B. *Inorg. Chem.* **1984**, *23*, 1440–1445.

(27) (a) Perrin, D. D. *Dissociation Constants of Organic Bases in Aqueous Solution*; Butterworths: London, 1972. (b) Guven, A. *Int. J. Mol. Sci.* **2005**, *6*, 257–275.

Table 1. Electronic Transitions of Ru(II) Complexes in CH₃CN at Room Temperature^a

complex	λ , nm (ϵ , mol ⁻¹ L cm ⁻¹)			
	LC; $\pi \rightarrow \pi^*$		MLCT; $d_{\pi} \rightarrow \pi^*$	LMCT; $\pi \rightarrow d_{\pi}$
[Ru(bpy) ₃] ²⁺	238 (30000) 250 (25000) 286 (87000)	323 ^{sh} (6900) 345 (4500)	420 (8035) 451 (9800)	
[RuCl ₂ (bpy) ₂]	240 (23750) 294 (90000)	375 (9703)	475 ^{sh} (5100)	524 (7887) 551 (9703)
complex 3	242 (31807) 292 (42055)	328 (14768)	431 ^{sh} (7220)	464 (8119)
complex 2	242 (40836) 292 (90000)	342 (16367)	460 (10247)	498 (9762)

^a sh = shoulder.**Table 2.** Photophysical Properties of Complexes **2** and **3** and Related Bipyridine Ru(II) Complexes

complex	solvent	λ	τ_{em} (ns)	ϕ_{em}	ΔE (abs - em)	$10^{-4} k_r$ (s ⁻¹)	$10^{-6} k_{nr}$ (s ⁻¹)	E_a (cm ⁻¹)
[RuCl ₂ (bpy) ₂]	CH ₃ CN	no luminescence						
[Ru(bpy) ₃] ²⁺	CH ₃ CN	598	870	0.061	5400	7.1	1.08	850
complex 3	CH ₃ CN	no luminescence						
complex 2	CH ₃ CN	594	650	0.0015	5100	0.23	1.54	987
	H ₂ O	591	509	0.0012	6000	0.23	1.96	

(bpy)₂(3Amnp)(CH₃CN)]²⁺ and *cis*-[Ru(bpy)₂(CH₃CN)₂]²⁺ in a stepwise fashion under continuous photolysis.

This pattern suggests that the 3Amnp labilization may result from the population of a dissociative excited state or an excited state with a relatively low barrier for dissociation. A likely candidate would be the mixed $d-\pi^*/d-d$ state. In addition, the 3Amnp ligand is a relatively weak-field ligand.²⁸ Therefore, it might be labile in metal complexes with low-energy MC excited states, as in the case of Ru(II) hexacoordinate complexes.²⁶

In contrast, complex **2** appears to be photochemically unreactive. No detectable UV-vis spectral changes could be observed after 2 h. The lack of photoreaction in solution for complex **2** is a consequence of the chelate ring of **1**, which contributes to the stability of the complex **2** under continuous light irradiation.

Luminescence Investigations. The emission maxima (λ_{max} , em), quantum yield (ϕ_{em}), and lifetimes (τ_{em}) measured for the photostable complex **2** and related complexes²⁸ are listed in Table 2 and Figures 4 and 5.

The emission band of complex **2** is broad and structureless, even in sucrose film, as illustrated in Figure 5. Figure 4 and Table 2 show that complex **2** exhibits a large Stokes shift similar to that observed for analogous complexes.²⁹

Whereas the emission spectra of complex **2** were independent of the excitation wavelength, between 260 and 550 nm, under the same circumstances the related complex **3** shows no luminescence.

These results indicate that the emission originates from the lowest excited state, which can be populated by either a direct optical excitation or an efficient internal conversion from higher charge transfer states.

A comparison between the absorption and the emission spectra of [Ru(bpy)₃]²⁺ and **2** is of interest here, since the same orbital will be involved in the absorption and emission of these complexes.

Figure 6 shows the absorption spectrum of [Ru(bpy)₃]²⁺ and the emission and excitation spectrum of **2**. The excitation spectrum of **2** measured by monitoring the emission at 590 nm matches perfectly the absorption spectrum of [Ru(bpy)₃]²⁺, indicating that the emission of **2** around 600 nm possesses an MLCT character from the bipyridine ligand.³⁰

It is interesting to note that replacing bpy by 3Amdpy₂-oxaNBE in the [Ru(bpy)₃]²⁺ causes a decrease in the emission lifetime; however, the Stokes shifts are unaffected (Tables 1 and 2).

As shown in Figure 7, the emission of complex **2** in CH₃CN increases in intensity upon lowering the temperature, and the emission quantum yield increased with decreasing temperature. At the lowest temperature studied (77 K), $\phi_{em} = 0.22$, while at room temperature is $\phi_{em} = 0.0015$.

Table 2 shows the lifetime decay for complex **2** in deaerated H₂O and CH₃CN solutions at room temperature. The τ_{em} versus T data could be fitted by eq $1/\tau_{em} = k' + A \exp(-E_a/RT)$ ^{28,31} with correlation coefficient of 0.975 (Figure 7, insert). The k_r , k_{nr} , and E_a values are summarized in Table 2. On the basis of the model proposed for [Ru(bpy)₃]²⁺ and developed by Crosby,³¹ the lowest-energy MLCT triplet is coupled to the ground state and to one higher-lying triplet state. Crosby³¹ suggested that emission occurs from a cluster

(28) (a) Caspar, J. V.; Meyer, T. J. *Inorg. Chem.* **1983**, *22*, 2444–2453. (b) Durham, B.; Caspar, J. V.; Nagle, J. K.; Meyer, T. J. *J. Am. Chem. Soc.* **1982**, *104*, 4803–4810. (c) Watts, R. J. *J. Chem. Educ.* **1983**, *60*, 834–842.

(29) (a) Villegas, J. M.; Stoyanov, S. R.; Rillema, D. P. *Inorg. Chem.* **2002**, *41*, 6688–6694. (b) Tyson, D. S.; Luman, C. R.; Zhou, X. L.; Castellano, F. N. *Inorg. Chem.* **2001**, *40*, 4063–4071.

(30) One of the reviewers made the following comment: “the interpretation of Figure 6, may be correct, but the presence of a [Ru(bpy)₃]²⁺ impurity participating in the emission can not be ruled out”. The reviewer argues “[Ru(bpy)₃]²⁺ compounds are very stable and favored, and tend to form as an impurity in the synthesis of [RuCl₂(bpy)₂]²⁺ from RuCl₃, even under careful stoichiometric control”. However, our deduction that the emission showed in Figure 6 is related to the presence of compound **2** in solution is maintained by analogy with both emission quantum yield and lifetime values that are smaller than those values found for [Ru(bpy)₃]²⁺ (see Table 2).

(31) (a) Hager, G. D.; Crosby, G. A. *J. Am. Chem. Soc.* **1975**, *97*, 7031–7037. (b) Hager, G. D.; Watts, R. J.; Crosby, G. A. *J. Am. Chem. Soc.* **1975**, *97*, 7042–7048.

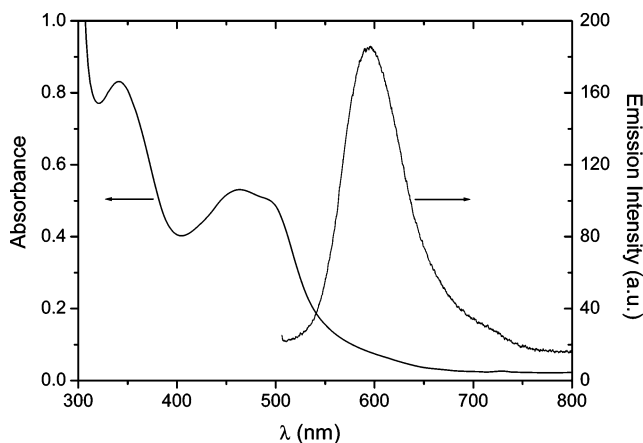


Figure 4. Absorption and emission spectra of complex **2** in CH_3CN .

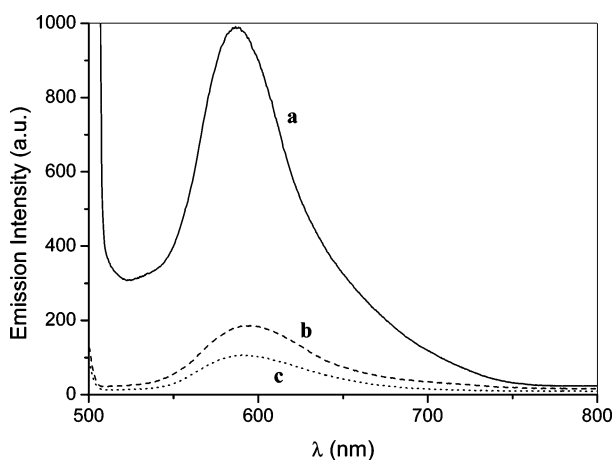


Figure 5. Emission spectra of complex **2** in sucrose film (a), CH_3CN (b), and H_2O (c) at room temperature.

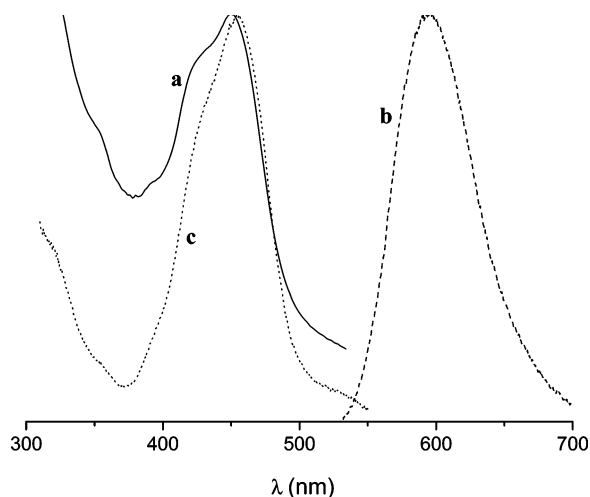


Figure 6. Normalized absorption spectrum of $[\text{Ru}(\text{bpy})_3]^{2+}$ (a) and normalized emission (b; $\lambda_{\text{exc}} = 450 \text{ nm}$) and excitation (c; $\lambda_{\text{em}} = 590 \text{ nm}$) spectra of complex **2** in CH_3CN .

of closely spaced levels ($\Delta E = 100 \text{ cm}^{-1}$), having similar but not identical properties. It is noteworthy that for complex **2** the access to this triplet state involves crossing a barrier of 987 cm^{-1} . According to previous works,³¹ the uppermost triplet state is assumed to be an MC state strongly coupled to the ground state.

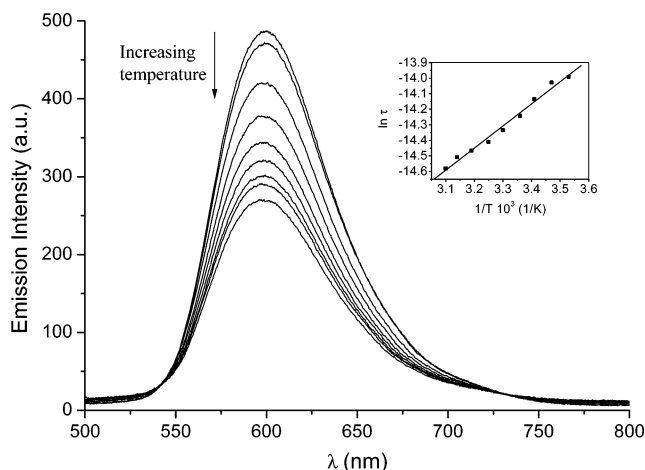


Figure 7. Emission decrease of complex **2** when increasing the temperature (10.0, 15.0, 20.0, 25.0, 30.0, 35.0, 40.0, 45.0, and 50.0 °C) in CH_3CN . Insert: Arrhenius plot for τ data.

Though complex **2** is sufficiently photoinert at ambient temperature for exploitation as photosensitizer of photoredox and energy transfer processes, related complex **3** is photo-reactive, and the presence of nearby MC states is responsible for such photolability.

The emission lifetime is mainly determined by the rate constant of the nonradiative decay, k_{nr} , which decreases by a factor of 31 on going from bpy to 3Amdpy₂oxaNBE in $[\text{Ru}(\text{bpy})_3]^{2+}$. This order reflects the decreasing $\text{Ru} \rightarrow \text{bpy} \pi$ -back-donation. Many factors can effectively contribute to the nonradiative deactivation of the MLCT excited state of **2**, such as the increasing mixing of $d_{\pi}(\text{Ru})$ and $\pi^*(\text{bpy})/\pi^*(3\text{Amdpy}_2\text{oxaNBE})$ orbitals. Also, the increased flexibility of the 3AmdpyoxaNBE ligand and the extensive delocalization within the Ru-(3Amdpy₂oxaNBE) chelate ring may provide efficient nonradiative deactivation pathways.

The lifetime in CH_3CN or H_2O solution suggested that complex **2** should be well suited for the investigation of photoinduced redox processes in large molecular assemblies.

Quenching Reactions. In order to understand the chemical properties of complex **2** in its excited state, the oxidative emission quenching by methylviologen (MV^{2+}) and $[\text{RuCl}(\text{NH}_3)_5]^{2+}$ ions were investigated.

These quenchers afford linear Stern–Volmer plots (ϕ_0/ϕ vs quencher concentration),³² indicating the bimolecular character of the quenching reactions. The bimolecular rate constants, k_q , were calculated from the slopes k_{SV} of the Stern–Volmer plots ($k_q = k_{\text{SV}}/\tau_0$; $\tau_0 = 509 \text{ ns}$). The values of k_q were lower than those controlled by diffusion (1.3×10^8 for MV^{2+} and $1.2 \times 10^8 \text{ mol}^{-1} \text{ L s}^{-1}$ for $[\text{RuCl}(\text{NH}_3)_5]^{2+}$), and lower than previously estimated for $[\text{Ru}(\text{bpy})_3]^{2+}$ ($2.4 \times 10^9 \text{ mol}^{-1} \text{ L s}^{-1}$ for MV^{2+}).³³

Laser Flash Photolysis Experiments. Figure 8 shows spectral and kinetic results for complex **2** in water after

(32) Bock, C. R.; Connor, J. A.; Gutierrez, A. R.; Meyer, T. J.; Whitten, D. G.; Sullivan, B. P.; Nagle, J. K. *J. Am. Chem. Soc.* **1979**, *101*, 4815–4824.

(33) Mahon, C.; Reynolds, W. L. *Inorg. Chem.* **1967**, *6*, 1927–1928.

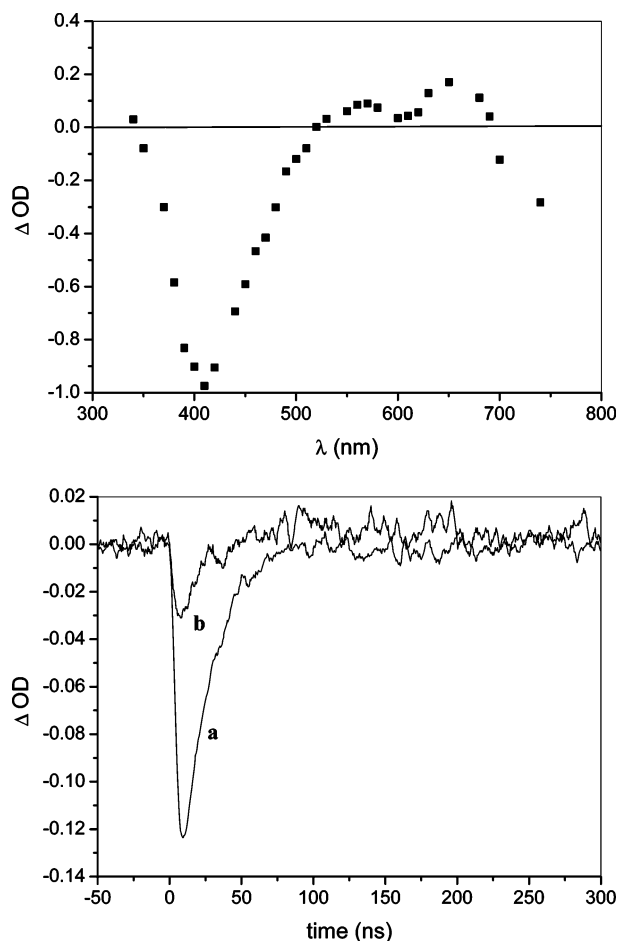


Figure 8. Transient difference spectra and kinetics for complex **2** in H₂O (1.5×10^{-5} mol L⁻¹). Upper: Difference spectra recorded 10 ns after 355 nm laser excitation. Lower: Decays recorded at 390 (a) and 480 (b) nm.

excitation with an 8 ns pulse at 355 nm. The kinetics was monitored at 390 and 480 nm, and the difference spectrum was recorded 10 ns after photoexcitation. The transient absorbance measurements of **2** ($27 \mu\text{mol L}^{-1}$) led to strong transient bleaching between 350 and 480 nm. Although at 390 nm the transient exhibited a large ΔOD , for both wavelengths studied (390 and 480 nm), the initial bleach decayed to the original baseline. The ground-state repopulation could be fitted to simple exponential decay $k_{\text{obs}} = 5.3 \pm 0.9 \times 10^7 \text{ s}^{-1}$ at 390 nm and $8.3 \pm 0.9 \times 10^7 \text{ s}^{-1}$ at 480 nm. Studies of $[\text{Ru}(\text{bpy})_3]^{2+}$ complex have shown that the MLCT excited-state spectrum can be modeled in terms of $\{\text{M}^{\text{III}} \text{bpy}^*\}$ chromophore³⁴ with bpy^* intraligand transitions providing a distinctive signature. Complex **2** (Figure 8) strongly resembles $[\text{Ru}(\text{bpy})_3]^{2+}$ (the MLCT state of $[\text{Ru}(\text{bpy})_3]^{2+}$), especially in the intense ~ 390 nm band. Thus, the expected MLCT character of the nanosecond excited state of complex **2** is supported by the nanosecond spectral data.

When such studies were performed in aqueous solutions equilibrated with MV^{2+} ($1.6\text{--}7.4 \text{ mmol L}^{-1}$), Figure 9, the magnitude of long-lived absorbance change measured at 390

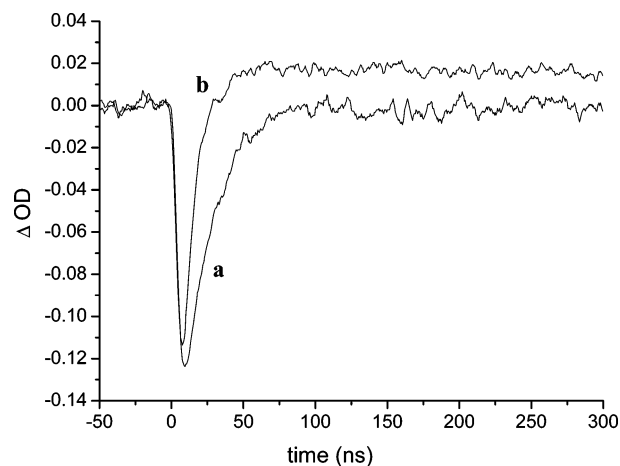


Figure 9. Decays for complex **2** in H₂O (1.5×10^{-5} mol L⁻¹) recorded at 390 nm in the absence (a) and presence (b) of MV^{2+} ; 7.4 mmol L^{-1} .

nm decreased from the one seen in the absence of quencher, resulting in $k_{\text{obs}} = 1.0 \pm 0.2 \times 10^8 \text{ s}^{-1}$. Furthermore, Figure 9 also shows that the initial bleach evolved into a transient absorbance.

Theoretical Analysis. As the nature of the excited states that account for the photochemical properties of complex **2** depends on the character of the MOs involved in the excitations, a comprehensive description of the ground state MO composition of this complex is given. Bond distances and bond angles selected from the optimization of this molecule using two DFT/basis set combinations are listed in Table 3. For comparison, the X-ray results for 4-amino-pyridine (4Amppy) related complex structure are also listed.³⁵ The structure of **2** is presented in Figure 10. In general, the DFT procedures gave optimized structures where both Ru–N(bpy) and Ru–N(3Amdpy₂oxaNBE) distances agreed with the experimental data for the *cis*- $[\text{Ru}(\text{bpy})_2(4\text{Amppy})_2](\text{ClO}_4)_2$ complex. Moreover, the asymmetrical carbonyl array justifies the multisignals in the IR and NMR spectra.

Complex **2** shows one bpy molecule, one pyridine ring N atom of the other bpy, one pyridine ring N atom of 3Amdpy₂oxaNBE, and the Ru atom lying in the same plane. The other N-pyridine arm of 3Amdpy₂oxaNBE is *trans*-positioned to a pyridine unit of a bpy localized in the *z* axis. The coordination around the central Ru atom is nearly octahedral. The two N-pyridine atoms of the 3Amdpy₂oxaNBE form angles of ca. 172° with each one of the N-pyridine atoms of the bpy ligands that are *trans*-positioned.

Whereas the mean interatomic distances Ru–N(bpy) are not sensitive to the substitution of 4Amppy for 3Amdpy₂oxaNBE, the Ru–N(3Amdpy₂oxaNBE) distance based on the DFT calculation (2.2 Å) is somewhat longer than that found in *cis*- $[\text{Ru}(\text{bpy})_2(4\text{Amppy})_2]^{2+}$ based on the X-ray data (2.12 Å).³⁵ This may be attributed to the π -acceptor nature of the amide-substituted pyridine units in **1** increasing the π -electron competition. Furthermore, the angle (3Amdpy₂oxaNBE)N–Ru–N(3Amdpy₂oxaNBE), 96.5° , is larger than

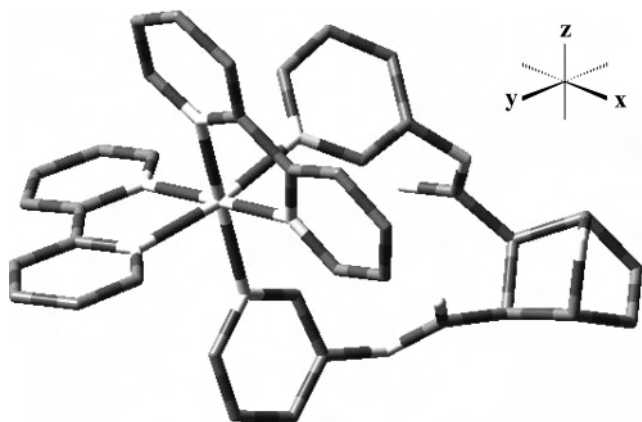
(34) Creutz, C.; Chou, M.; Netzel, T. L.; Okumura, M.; Sutin, N. *J. Am. Chem. Soc.* **1980**, *102*, 1309–1319.

(35) Chun-Ying, D.; Zhong-Lin, L.; Xiao-Zeng, Y.; Mak, T. C. W. *J. Coord. Chem.* **1999**, *46*, 301–312.

Table 3. Optimized Bond Lengths and Bond Angles in the Electronic Ground State of Complex **2** and the Comparison with X-ray Data for Related Complex

	X-ray data of <i>cis</i> -[Ru(bpy) ₂ (4Amnpy) ₂](ClO) ₂ ^a	optimized geometry of complex 2	
		3-21G	LANL2DZ
Bond Lengths (in Å)			
Ru— ^{eq} N(bpy; <i>trans</i> Apy)	2.060(1)	2.091	2.093
Ru— ^{eq} N(bpy)	2.070(1)	2.112	2.107
Ru— ^{ax} N(mer bpy)	2.076(1)	2.100	2.085
Ru— ^{eq} N(mer bpy)	2.057(1)	2.107	2.102
Ru— ^{ax} N(Apy)	2.104(1)	2.177	2.208
Ru— ^{eq} N(Apy)	2.121(1)	2.198	2.177
C(py ring)—N(amine or amide; ax Apy)	1.367(1)	1.428	1.432
C(py ring)—N(amine or amide; eq Apy)	1.366(1)	1.425	1.425
C(amide)—N(amide; ax Apy)		1.385	1.391
C(amide)—N(amide; eq Apy)		1.372	1.389
Bond Angles (deg)			
N—Ru—N (eq bpy bite angle)	80.0(1)	78.4	78.3
N—Ru—N(mer bpy bite angle)	78.7(1)	78.0	78.6
N—Ru—N (ax/eq Apy's expected bite angle)	91.7(1)	97.4	96.5
^{eq} N(bpy)—Ru— ^{eq} N(bpy)	173.3(1)	175.9	175.8
^{ax} N(Apy)—Ru— ^{ax} N(bpy)	175.8(1)	170.7	173.4
^{eq} N(Apy)—Ru— ^{eq} N(bpy)	176.0(1)	171.1	172.0

^a Reference 34; eq = equatorial (one or two py N's on *xy* plane); ax = axial (py N on *z* axis); mer = meridional (two py N's on *yz* or *xz* plane); Apy = 3Amnpy unit in **1** or 4Amnpy.

**Figure 10.** Final molecular geometry of complex **2** optimized by using density functional theory (DFT).

the one found for N(bpy)—Ru—N(bpy), 78°, reflecting the large hole size of the 3Amnpy₂oxaNBE ligand.

The large bite ring could explain the reason why the two py rings of 3Amnpy₂oxaNBE are not in the same plane, contrary to the bpy molecule. This lack of symmetry is experimentally supported by the increasing absorption at ca. 350 nm, going from [Ru(bpy)₃]²⁺ to complex **2** (Table 1; Figure 1).

Molecular Orbital Analysis. The MO composition of complex **2** is given in Table 4. The LUMO and the two following empty MOs, LUMO + 1 and LUMO + 2, have 100% 3Amnpy₂oxaNBE π^* and more than 90% bpy π^* character, respectively. In the same way, instead of a single HOMO, there are three close-lying highest occupied orbitals, which give rise to degenerated orbitals in the related complex³⁶ [Ru(bpy)₃]²⁺. Those MOs are a combination of bpy π and ruthenium d orbitals, which have an antibonding

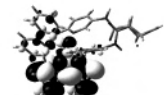
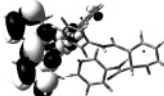
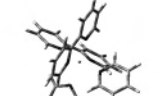


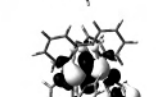
π interaction. Their energies are ~ 3 eV below the set of π^* orbitals of 3Amnpy₂oxaNBE and bpy ligands. Therefore, besides d—d (Ru) and MLCT (Ru \rightarrow 3Amnpy₂oxaNBE) bands, we can also expect MLCT (Ru \rightarrow bpy) and LLCT (3Amnpy₂oxaNBE \rightarrow bpy) transitions.

In the previous section, the lowest energy absorptions bands of complex **2** at 498 (2.5 eV) and 460 (2.7 eV) nm were assigned as a contribution from both metal to ligand ($d_{\pi} \rightarrow$ 3Amnpy₂oxaNBE) and ($d_{\pi} \rightarrow$ bpy) charge-transfer MLCT transitions, respectively. This assignment was based on the high intensity of the band, its solvatochromism (H₂O, $\lambda_{\text{abs}} = 468$; CH₂Cl₂, $\lambda_{\text{abs}} = 503$ nm), ligand dependence of its position, and comparison with related complexes: see Table 2. According to the MO diagram (Table 4), the main transitions of the first and second absorption bands originate from the highest filled metal d_{π} orbitals to the π^* orbital of 3Amnpy₂oxaNBE (3.2 eV) and bpy (3.4 eV), respectively. Both assignments are in agreement with the CT character of these absorption bands.

The above results show that the two homologous complexes **2** and **3** undergo different primary photoprocesses upon irradiation into their lowest-energy absorption bands. Complex **3** loses 3Amnpy, and **2** shows a strong luminescence similar to the one found for [Ru(bpy)₃]²⁺, which is a remarkable photoprocess for a pyridine based complex. The occurrence of a 3Amnpy-loss reaction is expected, since a similar reaction has been observed for related Ru complexes, such as *cis*-[Ru(bpy)₂L₂] (L = py; and substituted pyridines).²⁶ For these complexes, the efficiency of the photoreaction appeared to depend on the substitution of pyridine and on the energy difference between the MLCT and MC states.²⁶ The photoreaction was therefore proposed to proceed from the lowest MC state, after surface crossing from the MLCT states.²⁶ This is associated with the chelating nature of the 3Amnpy₂oxaNBE ligand present in **2**. A similar

(36) Daul, C.; Baerends, E. V.; Vernooijs, P. *Inorg. Chem.* **1994**, *33*, 3538–3543.

Table 4. Characters, Energies, and Countour Plots of LUMOs and HOMOs of Complex **2** Calculated by DFT

Orbital	Orbital character	Energy (eV)	Contour plot
Lumo+2	93% $\pi^*(\text{bpy})$	-7.4	
Lumo+1	96% $\pi^*(\text{bpy})$	-7.5	
Lumo	100% $\pi^*(\mathbf{1})$	-7.7	
Homo	82% $d_{xz}, d_{x^2-y^2}(\text{Ru})$; 12% $\pi^*(\text{bpy})$; 4% $\pi^*(\mathbf{1})$	-10.9	
Homo-1	42% $d_{yz}(\text{Ru})$; 17% $\pi^*(\text{bpy})$; 9% $\pi^*(\mathbf{1})$	-11.0	
Homo-2	45% $d_{x^2-y^2}(\text{Ru})$; 23% $\pi(\text{bpy})$	-11.0	

mechanism may explain the photochemistry of **3**. Concerning complex **2**, the first absorption band shifts to shorter wavelengths, and the lowest excited state decreases in energy with respect to the relative MC states and approximates its energy to the $d_{\pi} \rightarrow \text{bpy}$ CT transition. As a result, complex **2** does not show a release of the 3Amdpy moiety, but it shows luminescence similar to the one found in $[\text{Ru}(\text{bpy})_3]^{2+}$.

For the interpretation of these effects, we have to consider the character of the orbitals involved in the electronic transitions and the nature of the lowest excited states of these complexes. The emissive lowest-lying excited state in the $[\text{Ru}(\text{bpy})_3]^{2+}$ complex originates from electron excitation of the d_{π} antibonding orbital of the metal to the π^* -orbital of the bpy ligand. The thermally activated decay of the excited state of $[\text{Ru}(\text{bpy})_3]^{2+}$ has been ascribed to a thermal population of a reactive d–d state.²⁸ Due to the coordination of the relative weak-field 3Amdpy₂oxaNBE complex are expected to lie lower in energy than those of $[\text{Ru}(\text{bpy})_3]^{2+}$. Therefore, the MC states are expected to occur at lower energy, thermally accessible from the lowest CT state, explaining the photo-

chemical activity of the bis(3Amdpy) complex. The temperature dependence of the excited-state lifetime may be better explained by deactivation through a close-lying higher charge transfer state.

Conclusions

The complex **2** ion constitutes a new class of emissive transition metal complex with long-lived excited states of a charge-transfer character. The oxidative quenching experiments show that this complex may be considered an electron-transfer sensitizer and/or catalyst in photochemical reductions and it could be used as a building block for the construction of photochemically active redox molecular devices.

Acknowledgment. The authors would like to acknowledge the financial support from FAPESP, CAPES, and CNPq. They are also indebted to Dr. Amando Siuiti Ito from FFCLRP-USP for supplying the equipment for fluorescence lifetime measurements and Angela Cristina Pregnolato Giampedro for reading this manuscript.

IC062478V